Biosensors and Bioelectronics 137 (2019) 263–270

Contents lists available at ScienceDirect

Biosensors and Bioelectronics

journal homepage: www.elsevier.com/locate/bios

In situ terminus-regulated DNA hydrogelation for ultrasensitive on-chip microRNA assay

Shengyuan Deng[a,1], Juan Yan[b,1], Fei Wang[c,e], Yan Su[d], Xueli Zhang[c], Qian Li[e], Guang Liu[a], Chunhai Fan[e], Hao Pei[f,**], Ying Wan[d,*]

[a] School of Environmental and Biological and Engineering, Nanjing University of Science and Technology, Nanjing, 210094, China
[b] College of Food Science and Technology, Shanghai Ocean University, Shanghai, 201306, China
[c] Joint Research Centre for Precision Medicine, Shanghai Jiao Tong University & Affiliated Sixth People's Hospital South Campus, Fengxian Hospital, Shanghai, 201499, China
[d] School of Mechanical Engineering, Nanjing University of Science and Engineering, Nanjing, 210094, China
[e] School of Chemistry and Chemical Engineering, Shanghai Jiao Tong University, Shanghai, 200240, China
[f] Shanghai Key Laboratory of Green Chemistry and Chemical Processes, School of Chemistry and Molecular Engineering, East China Normal University, Shanghai, 200241, China

ARTICLE INFO

Keywords:
Non-template isothermal amplification
Terminal deoxynucleotidyl transferase
DNA hydrogel
Electrochemical miRNA assay
Microarray sensor

ABSTRACT

In this work, a dynamic terminus-regulated fabric of DNA hydrogel was invented in debt to the reiterative catalysis of terminal deoxynucleotidyl transferase (TdT). It extended free 3'−OH end to an overhang of homopolymeric adenosine base pair, and alternated with branching from the frayed complementary seed oligo $T_{20}G_5$. The cycle of this template-independent and isothermal amplification resulted in a microscale dendritic DNA fractal at first, which then gelatinized into a cohesive and intricate 3D network. Details of the complex were elucidated with gel electrophoresis, confocal and atomic force microscopy. Its well hydrated inner space could further provide plenty of biocompatible chambers for enzymatic transducers fused along the elongation. Taking merits of this neat and flexible setup, an *in situ* hydrogelation strategy was developed and utilized in the signal cascade of a miRNA biomarker detector on an electrode microarray, thus accomplished an ultrasensitive, selective and high-throughput sensing even for real samples. This collective manipulation of DNA-protein hydrogel ensemble on interface demonstrates its potency as a general scheme of sensitization in bioanalytical applications.

1. Introduction

Owing to its unique programmability, DNA has now been established as a miscellaneous building block for configuring novel structures such as nanomachinery, automaton, origami, and kirigami (Bath and Turberfield, 2007; Hong et al., 2017; Rothemund, 2006; Thomas et al., 2011; Xiong et al., 2013). As been foretold in the pioneering work by Seeman, combining the previous feature with the inborn bio-compatibility and hydrophilicity further grants these DNA-scaffolded artefacts full access to super vigorous biomedical applications (Qu et al., 2017; Seeman, 2003, 2010; Wei et al., 2018; Winfree et al., 1998), for typical example, customized DNA cargo holds of stimuli-responsive allostery for targeted drug delivery and gene unloading (Li et al., 2015b), platonic polyhedral DNA transducers of strong protein repellence for highly sensitive cytosensing and immunofluorescence, *etc.* (Ge et al., 2014; Pei et al. 2010, 2011; Wen et al., 2012; Zhou et al., 2014). Moreover, DNA-templated poly-peptide and polycrystalline hybrids were even brought into being for *in situ* multilayered tissue printing(Li et al., 2015a; Liu et al., 2018). Such sol-gel formation literally benefits from the manipulable ductility and the subtle tacticity of DNA backbones, being essentially a particular type of hydrogels not only with all the above merits but more functionally bulky and scalable in real practice.

The potential in mass production of relatively huge nucleotide ensembles motivated scientists to develop specific paradigms for synthetic hydrogels (Li et al., 2016). Initial strategies preferentially adapt the LEGO idea for piecing tiles of single-strand (ssDNA) or duplex together into a hierarchical three-dimensional grid (Fu et al., 2013; Goodman et al., 2005; Wei et al., 2012). Despite the high precision plus an aesthetic value, this method barely has any fault tolerance in terms of

* Corresponding author.
** Corresponding author.
E-mail addresses: peihao@chem.ecnu.edu.cn (H. Pei), wanying@njust.edu.cn (Y. Wan).
[1] These authors contributed equally to this work.

https://doi.org/10.1016/j.bios.2019.04.053
Received 16 March 2019; Received in revised form 24 April 2019; Accepted 29 April 2019
Available online 03 May 2019
0956-5663/

sequence design, while too skill-intensive would be another downside. To circumvent this issue, ssDNA-pendent copolymers were recruited as a simpler crosslinking alternative (Li et al., 2012; Nagahara and Matsuda, 1996). As such, exogenous triggers like pH, cation and photon then came in handy to regulate the gelation degree (Liao et al., 2017; Lu et al., 2012; Weiwei et al., 2014). Later on, this way of real-time growth got evolved to be more efficient and neater with recourse to enzymes, *e.g.* polymerase and ligase-catalysed networking among branched bricks (Um et al., 2006), and the rolling circle amplification (RCA)-interdigitated molecular padlocks (Lee et al., 2015). Clearly, these biocatalyses fulfilled a high cost performance in a resource (primer)-limited context. − A trait quite matches the applicative scenarios of biosensors.

Herein, to explore the capacity of catalytic DNA hydrogels in miniaturized electrochemical microarray, an isothermal catalyst - terminal deoxynucleotidyl transferase (TdT), specialized for casual mononucleotide (dNTPs) coupling (Wan et al. 2013, 2014, 2015; Wang et al., 2016), was exploited to direct the on-site sprawl of hydrogel in a non-template manner. After hybridization with targets, the exposed 3'−OH in capture probes was tailed and extended by TdT-mobilized feeds of dATP or its fluorophore-tagged (dATP*) or biotinylated (bio-dATP) replacements, followed by self-multi-furcation with short oligos of $T_{20}G_5$ seeds (Scheme 1). Through cycles, a 3D microscale hydrogel containing refined dendritic fractal spawned on the substrate. Such divergent morphology was corroborated by electrophoresis, confocal and atomic force microscopy. More importantly, it facilitated a simultaneous fusion of high-density labelling avidin conjugated horseradish peroxidase (Av-HRP) inside the well hydrated jelly, which also preserves the natural conformation and activity. Using a cancer biomarker microRNA (hsa-let-7d-5p) as a model analyte, this methodology enabled its sensitive and selective detection down to femtomolar with facile protocol and sensing setup. Hence, this work would demonstrate the potency of DNA hydrogels, thriving on TdT reaction, in signal enhancement of bioassays.

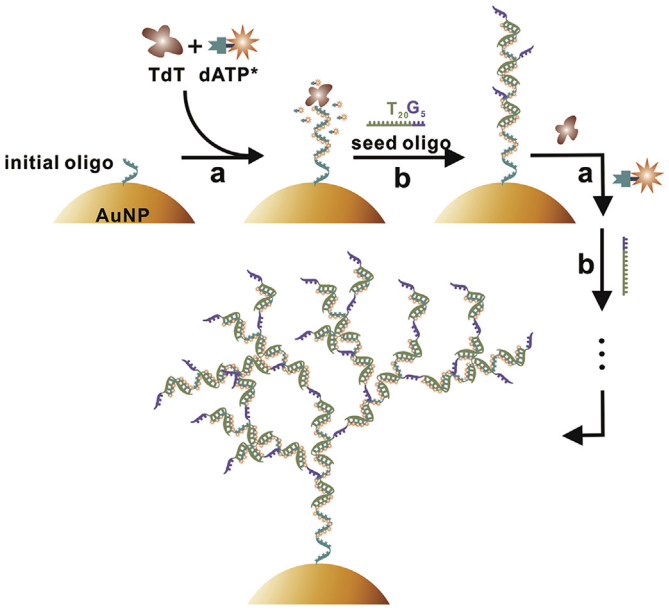

Scheme 1. Schematic illustration depicting the growth of a treelike DNA hydrogel in an enzyme-driven cycle on a single gold nanoparticle (AuNP) surface, a microscopic representative of the local curvature on a gilded microchip.

2. Material and methods

2.1. Materials and reagents

DNA and RNA oligonucleotides were purchased from TAKARA Biotechnology with sequences in Table S1 of the Supplementary Information (SI). Tris(hydroxymethyl)aminomethane (Tris) was ordered from Cxbio Biotechnology. Ethylenediaminetetraacetic acid (EDTA), *R*,*ω*-alkanedithiol dithiothreitol (DTT), and 6-mercapto-1-hexanol (MCH) were procured from Sigma-Aldrich. 3,3′,5,5′-tetramethylbenzidine (TMB, Neogen K-blue, low-activity substrate), avidin-conjugated horseradish peroxidase (Av-HRP), terminal deoxynucleotidyl transferase (TdT), fluorescein isothiocyanate-tagged as well as biotinylated deoxy-adenosine triphosphate (dATP* and Bio-dATP), and gold nanoparticles (AuNPs) (Average Size: 15 ± 2 nm, Optical Density = 1) were bought from Neogen, Roche Diagnostics, MBI Fermentas, Beyotime Biotechnology, and Cytodiagnostics, respectively. All solutions were prepared with Milli-Q ultrapure water (≥18 MΩ·cm) from a Millipore purification system. Their components and usages are listed as follows: 10 mM pH 7.4 Tris-EDTA (TE) buffer containing 1 M NaCl for hybridization, 10 mM pH 7.4 Tris-HCl for E-DNA detection, 20 mM pH 8.0 Tris-HCl plus 50 mM $MgCl_2$ (TM) for DNA immobilization, 0.1 M pH 7.4 phosphate buffer saline (PBS) for rinsing, and 0.1 M pH 7.4 PBS including 0.5% casein for dilution of Av-HRP.

2.2. Biocatalytic development of DNA hydrogels on AuNPs

Initial oligos were immobilized upon the surface of an individual gold nanoparticle (AuNP) by referring to the reported protocol (Zhang et al., 2007). After DNA@AuNPs were synthesized, 100 μL of an aqueous mixture of adequate bio-dATP and 1 U (1 nmol of nucleotide polymerized per hour) TdT was added in to trigger the TdT-mediated extension at 37 °C over a typical period of 30 min (step a in Scheme 1). After repetitive separation under 10-min centrifuge at 12000 rpm and decanting the supernatant, 100 μL of seed strands (portion-wise) were introduced to the red precipitate, proceeding to heat up to 95 °C for 5-min incubation and a successive annealing to the ambient temperature for the partially complementary (cDNA) gratfing and branching (step b in Scheme 1). Reiterating step a and step b for several cycles, the product would then be ready for harvest and characterization.

2.3. Instrumentation

The nucleotides produced at different reaction stages were subjected to electrophoretic analysis in agarose gel (1% w/v) involving GelRed Nucleic Acid Stain (0.01% in water, 0.1 mL from Biotium), which was paralleled with 100 base-pair DNA ladder Marker (TAKARA Biotechnology) in pH 8.4 1 × TAE (Tris-Acetic-EDTA) buffer. The electrophoresis was carried out at a constant potential of 110 V at room temperature for 30 min, afterwards photographed by a Bio-Rad Laboratories Gel imaging system.

Atomic force microscopy (AFM) was employed to probe the morphology of hydrogel, the four-cycle product of which was diluted and drop-cast onto a freshly peeled mica sheet. After 5-min adsorption, the piece in interest was immersed in water and gently blown dry with N_2 stream. The topological images out of the ScanAsyst software were scanned across an area of 10 × 10 μm^2 in air mode on a Bioscope Resolve AFM (Bruker Inc., U.S.) with a high-precision normal spring cantilever of SNL-series silicon (Geometry: 100 × 100 × 15 μm^3, Resonant Frequency: 65 kHz, Elasticity: 0.35 N/m) under ambient condition. The nominal and the maximized tip radii are 2 and 12 nm, respectively.

Epifluorescence microscopic imaging was performed using a Leica TCS SP8 confocal laser scanning microscope with an enclosure system (OKOlab, Italy) for temperature, humidity, and mass flow controls. Dye-

labelled DNA hydrogel was excited with a 488 nm solid-state incident laser source. Optical signals in red channel were collected (through an air-dry objective with Numerical Aperture (N.A.): 0.9, Amplification: 63 ×), captured by a MicroMax 1024 CCD camera (Princeton Instruments) and processed with ImageJ (Universal Imaging). The programmed visualization was parameterized as a 20 min timelapse of snap-shots taken at an interval of 30 s (Auto Maximum Exposure: 250 ms, Camera Area: Full Chip, Scan Width: 10, Target Intensity: 65535, % of Max: 100).

2.4. Fabrication of sensing interface and electrochemical miRNA assay

The miRNA sensors were fabricated by complying with standard operating procedures in a literature (Wu et al., 2010). Briefly, 4 μL of thiolated capture probe at an appropriate concentration and 200 μM DTT were co-immobilized on a uniform gold electrode (Inner Diameter: 2.5 mm) microchip, followed by unspecific blocking with MCH to form a self-assembled monolayer (SAM) of SH− DNA/DTT + MCH. To finish each step, the working electrode was rinsed thoroughly with copious PBS and dried in N_2 atmosphere. Next, 4 μL of miRNA of various concentrations was pipetted onto the above interface and stands hybridizing for 60 min at room temperature. Again, the planar bulky electrode surfaces under-went extensive rinse and gas dryer prior to a similar *in situ* TdT-catalysed DNA netting as adapted from the session concerning the spherical AuNP regime. Finally, 4 μL of Av-HRP (0.5 U/mL) as multiple reporter units was mounted upon the foregoing modification, getting prepared for signal transduction.

Electrochemical measurements were conducted using Cuvette-1600 Multi-Channel Microfluidic Lab-on-Chips system (Fasteur Biotechnology, Beijing, China) installed with Grand Canyon Studio 1.1.13 package. The customized chips consist of an array of 16 sensors patterned from mask lithography, and each works independently and disposably as either a potentiostatic or a galvanic module of a compact three-electrode configuration, with working, reference, and counter electrodes (Fig. 2A).

3. Results and discussion

3.1. Mechanism on TdT-induced DNA hydrogel formation

Scheme 1 shows the progressive formation of partial hydrogel - one piece of dendron as a proof-of-concept illustration. To be specific, first of all, the so-called initial oligos were immobilized on the surface of AuNPs via the well-known bonding between 5'−SH terminal and Au (Zhang et al., 2007), the coverage of which was assumed to be uniform. Of note, here AuNP was employed as the carrier; its spherical surface as a catalysis bed would better manifest TdT capability and characterize its product rather than on a planar gold electrode.

In the second move, the introduction of TdT commenced the strand elongation at 3'−OH, which randomly picks 1 nt out of the multiplexed dNTP (N = A/T/C/G) reservoir at a time and links them sequentially (Tjong et al., 2011). In this sense, to avoid the occurrence of any stochastic addition, we chose dATP as the sole substance, thus resulting in overhangs of monotonic long poly(A) tail after the step a in Scheme 1. Presumably, given excessive dATP, a single-stranded extension like this would carry on and on, which indicates that the catalytic period of step a needs to optimize along with other relevant parameters for an overall balance among the epitaxy in all directions (isotropic stretches).

In the third place, a modified TdT-mediated chain reaction was realized by hybridizing poly(A) with short oligo $T_{20}G_5$, which behaved as multiple seedlings to render more frayed growing points. This procedure denotes step b. Alternating it with step a would change the linear growth pattern and burst it into an exponential one. Such a two-step iteration requires neither pre-defined primers or templates nor cryo-thaw cycle, still it could accomplish the same amplification effect as PCR, RCA and the hybridization chain reaction (HCR) (Ge et al., 2014; Yata et al., 2015). More than that, in view of binding sites on poly (A), the cascade in structural bifurcation would probably composes some dendritic landscape in a local region of interest, which together with the final product await to be identified further.

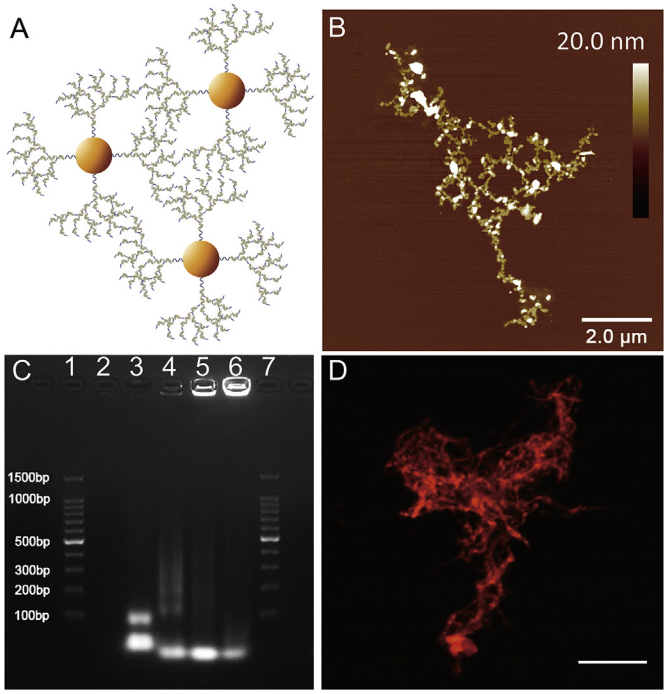

Fig. 1. Characterization of DNA hydrogel. (A) Schematic illustration of entanglement in a dendritic DNA network on AuNPs as a zoom-out version of the lower Scheme 1. **(B)** AFM topographic scan on a clean mica sheet holding dry product after 4 catalytic cycles on AuNPs. Scale bar: 2 μm. **(C)** A snapshot about the gel electrophoresis with lanes from left to right: (1) DNA ladder; (2) initial oligo; (3) to (6): products after 1st, 2nd, 3rd, and 4th round of reactions in the absence of AuNPs, respectively; (7) DNA ladder. **(D)** Confocal microscopic image of the product extended by FITC-dATP after a 4-cycle period. Scale bar: 10 μm.

3.2. Morphological characterization of DNA hydrogel

In order to validate the foregoing theoretical inference about enzymatic generation of DNA hydrogel, several techniques were applied to characterize the products at various stages.

The AFM topographic image in Fig. 1B exhibits a sampled web of DNA skeleton derived from four reaction rounds. This construction covers an area with a lateral size of around 6 μm and a color-coded thickness of less than 20 nm. By referring to the multiplied version of Scheme 1 in Fig. 1A, the bright spots in this geothermal map should belong to individual AuNPs (~15 nm) or residual TdT and their overlaps. Consequently, the light brownish serpentine trail corresponds to the collapsed DNA adsorption, which expands greatly across a distance of 8 μm between its upper left tip and the lower right. Although it appears as a mere projection with uneven roughness, the entire picture echoes very well with those imagined 3D networks. More significantly, the entangled dendrons in proximity actually encompass a good deal of relatively rigid space containing dense nucleic acids and concomitantly of strong hydration (Fig. 1A), both of which are considered as the prerequisites for gelatinization (Um et al., 2006). In this way, we have a direct piece of evidence on the successful fabrication of DNA hydrogel. It turns out to be a large ensemble of full-DNA dendrimers if analogous to the configuration of poly(amidoamine) (PAMAM) at its high generations (Li et al., 2000). Based upon the analysis of this AuNP-centred system, it is fair to believe a quite similar scene there on the electrode surface, however that would also rely upon the amount of targets.

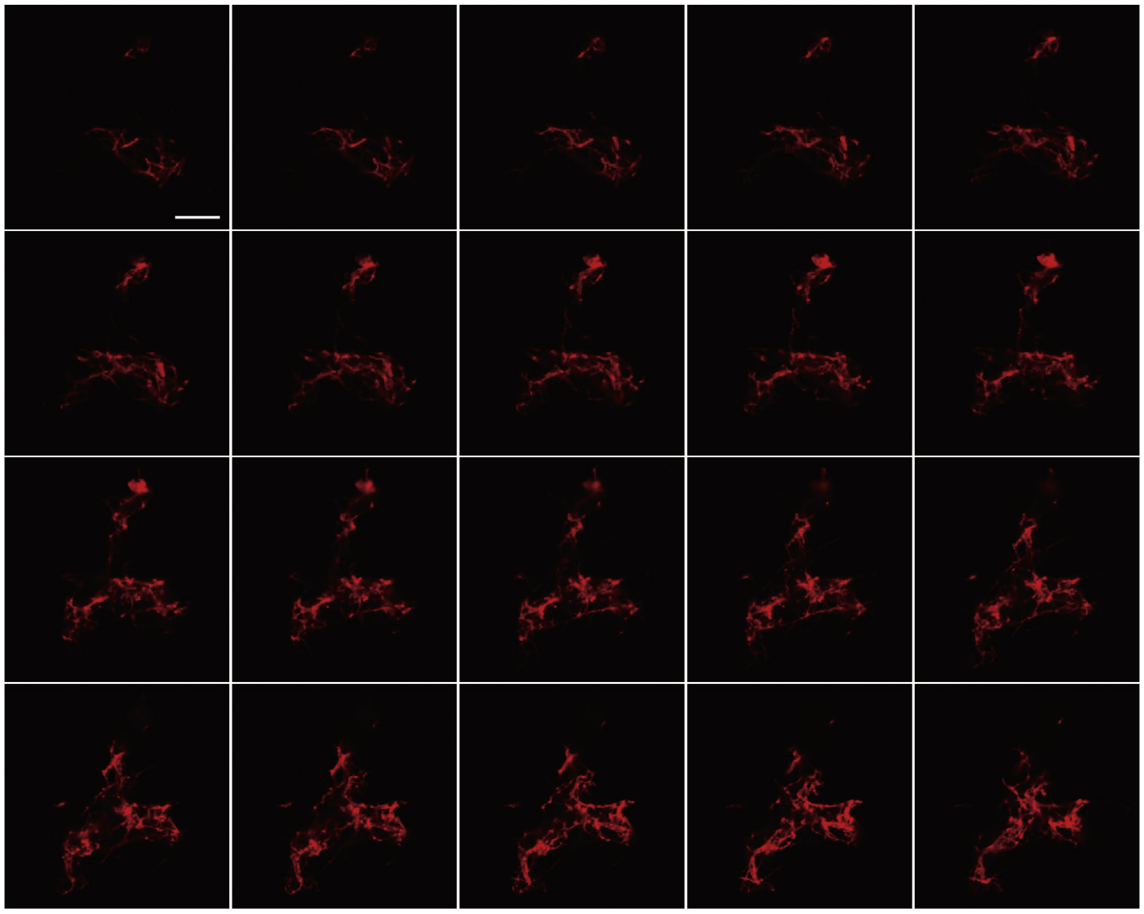

Fig. 2. *Z*-stack series of Fig. 1D. Images were collected at an interval of 0.97 μm in *z* distance by following a stepwise top-down order. Scale bar: 10 μm.

To prove the relationship between the production rate in TdT catalysis and the reaction progress, agarose gel electrophoresis was adopted by evaluating products extracted at consecutive cycle segments, *i.e.* Lane 3, 4, 5, 6 in Fig. 1C corresponding to 1st, 2nd, 3rd, 4th cycle, respectively, with respect to the molecular weights(Tjong et al., 2011). In all cases, the reactants of the same species were prepared in equimolar without AuNP. Lane 1 and 7 are reserved for markers. Apparently, there is no band for the initial strands in Lane 2 as the blank control. After the 1st "lengthen-and-graft" loop (Lane 3), two separated bands were observed, which stand for the elongated ssDNA (the lower one) and its complementary hybrid with seeds (the upper at 100 bp), respectively. As the cycler proceeded, products with increasingly longer base pairs emerged from 150 to 1000 bp, whose phoretic mobility became so low that was extremely retarded (Lane 4) and even stopped migrating at the inlet port (> 1500 bp in Lane 5 and 6). The latter implies the existence of superstructures in consistence with the scanned profile in Fig. 1B. By comparison among every distribution along the strips and the brightness at the entries, it is obvious that a series of DNA intermediates begin to take shape out of the 2nd cycle, whereas the individual product out of 4th drastically outweighs those previous. Possibly due to the kinetic change in steric hindrance, traces of oligo remnants are there; but as cycles accumulated, they decreased gradually. After all, as a semi-quantitative reflection of an eruptive growth in vitro, such evolution has been verified by electrophoresis, which could be explained by the principle detailed before. From this point, TdT can be designated as a growth assistant(Tjong et al., 2011), mean-while $T_{20}G_5$ plays as the growth factor.

Last but not the least, it would be compelling to display the realistic hydrogel at a tridimensional and larger scale. Instead of the indirect AFM visualization and the high-resolved superficial observations via the scanning electron microscopy (SEM) and the transmission (TEM) (Lee et al., 2012), confocal laser scanning microscopy was selected to catch both full sight and insight of the hydrogel. As displayed in Fig. 1D, the FITC label at dATP* is capable of illuminating the 4-cycle product in an aqueous environment, which spreads much wider over 30 × 30 μm^2 in contrast to the AuNP-supported regime (< 10 × 10 μm^2) in Fig. 1B. Therefore, immense textile with more intertwined texture can be weaved by free DNA, while it would not be so easy for DNA on colloids to do so if taking their slow diffusion into account. The former as a whole resembles the microfilament cytoskeleton; in the meantime, its surface tension as a consequence of wetting from confined water molecules tend to consolidate itself into a glassy state (Zhang et al., 2013). Indeed, such phase transition governs the formation of our designed DNA hydrogel (Ren et al., 2015).

The obtained 2D confocal image can be reconstructed along *z* axis into a stack (*z*-stack) of computed tomographic photos as merged in Fig. 2. By peering at the gradual rich details from the top left to the bottom right, a longitudinal distribution of DNA net can be verified, which is presented as a complex of vertical crossings, junctions and flyovers. According to stepping interval of 0.97 μm, the depth of this thin coating is estimated to be a couple of micrometers. Taking advantage of ImageJ, the 3D contour of this panel can be reconfigured into an angio-graphic slice as showcased in the revolving Movie M1, which confirms the solid dimension of resultant hydrogel. Its high surface-to-volume ratio, as a reminiscent of true modification on electrode, favours the incorporation of numerous reporting moieties into some prototypical devices (Wan et al., 2015), which may be promising to facilitate the signal improvement in biomarker detection.

Supplementary video related to this article can be found at https://doi.org/10.1016/j.bios.2019.04.053

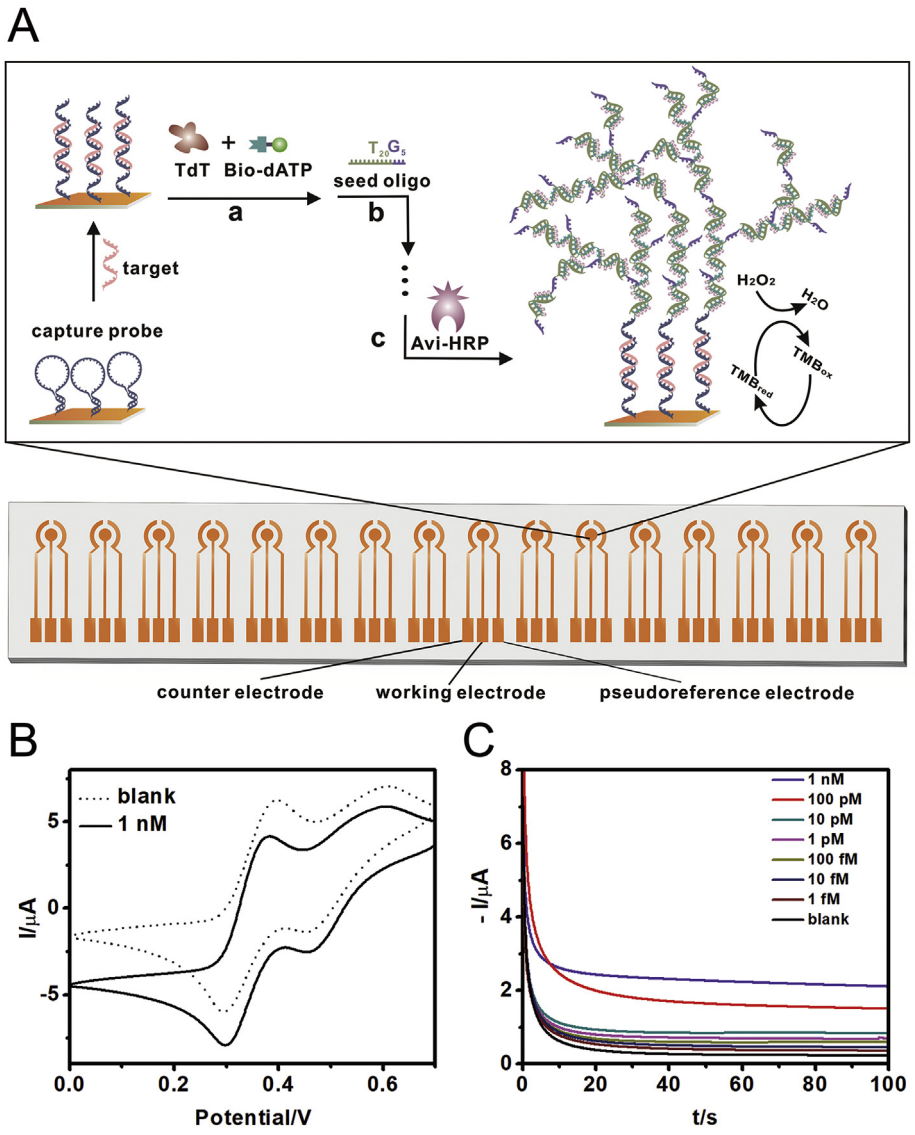

Fig. 3. Application of in situ DNA gelling strategy for miRNA sensing. (A) Schematic illustration of the sensing mechanism (upper panel) and the microarray platform (lower). **(B)** Typical cyclic voltammograms of the sensor during the detection of 1 nM (solid curve) and 0 M (dashed) target. Scan rate: 0.1 V/s. **(C)** The corresponding amperometric profiles at 0 (blank), 1, 10, 100 fM; 1, 10, 100 pM; and 1 nM (from bottom to top) on the potentiostatic condition (0.1 V).

3.3. Sensitized miRNA sensor by virtue of DNA hydrogel

The proposed TdT-driven gelling of DNA was transplanted in the sensor interface as a tentative approach of *in situ* polymerization and dissemination of biotransducers (Fig. 3A). To do it, 5'−thiolated stem-loop captures were assembled on the gold electrode. In absence of the target, the hairpin stayed folded with 3'−OH inaccessible to TdT. It then unfolded in presence of targets to reveal 3'−OH. Noteworthily, the target RNA may form hairpin structures with overhangs, in this case its binding would instead follow a strand replacement kinetics as described in literature (Ratajczak et al. 2018a, 2018b; Stobiecka and Chalupa, 2016). By implementing the aforementioned cyclic process, DNA network turned up rambling on the surface. One thing noteworthy is that, under this circumstance bio-dATP substituted dATP intentionally to supply the amplification when planting considerable biotins within. This action leaves spots for anchoring avidin-conjugated tracing tag (*e.g.* Av-HRP) in future. By rough calculation, 1 avidin (66–69 kDa) is tantamount to 100 bp (680 g/mol per bp) (Jain and Cheng, 2017). That is to say, in stoichiometry, one target recognition event would lead to a concerted reduction of H_2O_2 by tens of thousands of HRPs. Such greatly enhanced turn-over can pave a desirable signal-transduction pathway.

The feasibility of this strategy was challenged with an miRNA target: hsa-let-7d-5p, a prognostic and predictive marker for personalization of the cancer treatment in the peripheral whole blood (Maffioletti et al., 2016). A 16 micro-fabricated sensor array was engineered, each consisting a set of working, counter and pseudo-reference electrodes (Fig. 3A), to allow voltammetry and amperometry for multiplexing assay. In Fig. 3B, the cathodic current (i_c) at the reduction peak of 0.3 V augmented remarkably for 1 nM target (solid voltammogram), which is ascribed to the electro-reduction of the oxidized TMB (TMB_{ox}) as proton donor. It suggests the attachment of Av-HRP to the hydrogel just as we expected. Furthermore, by varying the target content, the current readings differ accordingly. As combined in Fig. 3C, chronoamperometric $i_c \sim t$ decay trace escalates steadily in response to the increasing quantity of analytes. Now the two variables seem to be well correlated. In light of this, systematic optimizations are needed preceding the establishment of a valid dependence.

Abiding by the control variate method, four elements: the cycle number, the density of capture probe, the concentration of seed DNA, and the time for elongation, were interrogated in orders (Basic set: 4, 1.0 μM, 1.0 μM, and 30 min) by means of the signal-to-noise ratio (s/n)

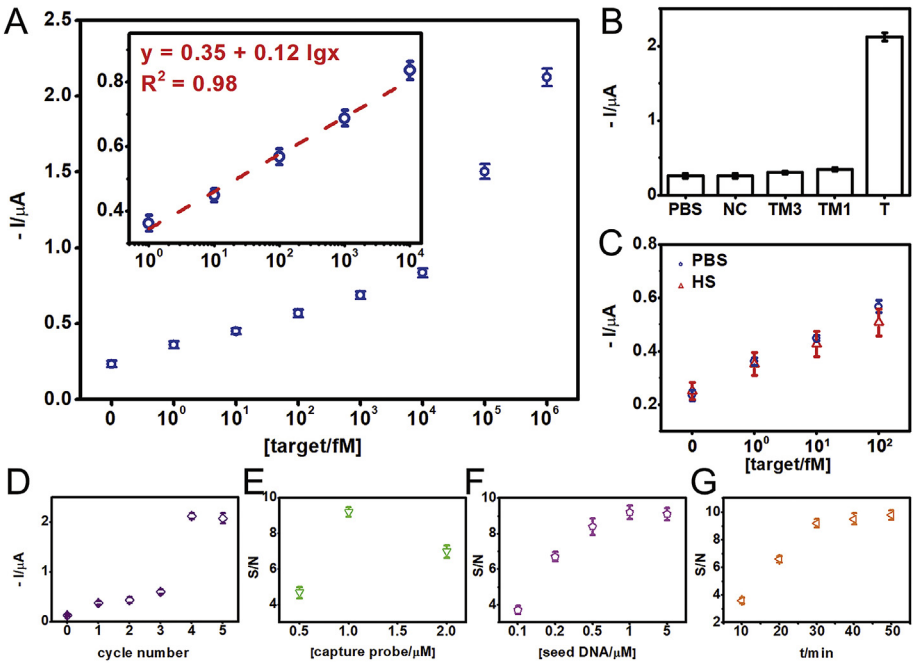

Fig. 4. miRNA sensing performance. (A) Amperometric response vs. logarithmical concentration of hsa-let-7d-5p. **Inset:** Calibration curve and its linear fit. **(B)** Histogram of selectivity testing results from 1 nM targets (from left to right): PBS as blank control, non-cognate DNA (NC), 3-base mismatch (TM3), 1-base mismatch (TM1), and perfect match (T). **(C)** Detection of targets dissolved in human serum (HS) as simulated real samples on the contrary to those aliquoted in buffer. **(D − G)** are the optimization of a variety of experimental conditions: **(D)** cycle number, **(E)** concentration of capture probe, **(F)** concentration of seed DNA, and **(G)** catalysis period for TdT. All data were collected from at least three independent runs in parallel.

defined as $s/n = I_{signal}/I_{blank}$, where I_{signal} and I_{blank} represent the amperometric signal at 1 nM and 0 M target, respectively. First and foremost, as we perceived above, the recurrence of step a + b decides the volume of hydrogel and the capacity of HRP. The real tendency was compiled in Fig. 4D, that i_c raises in the initial 3 repeats and accesses to a plateau at 4. Extra repetition did not contribute positively to i_c any more; conversely it drops a bit, indicative of a trade-off between the consumption of bio-dATP and the accessible biotins to Av-HRP. As such, 4-cycles is the optimal choice. Secondly, the dosage of the capture probe was adjusted by altering in a range from 0.5 to 2 μM. The highest s/n was found at a median of 1.0 μM (Fig. 4E), which also signifies a compromise between the densification of fibrous DNA network and the stereochemical crowding effect originated from the capture (Wan et al., 2014). As for the seed oligo, the s/n goes upward until a saturation at 1 μM(Fig. 4F). This phenomenon highlights a competitive binding among all $T_{20}G_5$ due its high content and long complementary domain. In the end, the duration for TdT incubation was tested, and 30 min is testified to be sufficient in Fig. 4G, which underscores that the apparent coverage of hydrogel and its complexity still dominate the signal output regardless of a fast catalytic turnover frequency of TdT towards the dATP monomer (180 ± 5 min^{-1}) (Tjong et al., 2011).

By completing parameter optimization, the best performance of the sensorgram can be reached. From it, a linear relevance was figured out between i_c and the logarithmic concentration of miRNA ranged from 1 fM to 10 pM, spanning at least 4 orders of magnitude (Fig. 4A inset). This proportional band is eligible to include the target expression level in major metabolism (Maffioletti et al., 2016). A calibration curve was fitted out with a regression equation of $y = 0.12 \cdot \log(x) + 0.35$ ($R^2 = 0.98$, y in μA and x in fM). The detection limit was assessed to be 0.35 fM (> 3 standard deviations). Additionally, there might be certain quasilinear between 10 pM and 1 nM so that 10 pM acts as the inflexion in such piecewise linearity. We speculated this attributed to higher opportunity of proximal bridging by $T_{20}G_5$ in the situation of more targets.

To inspect the selectivity of this sensor, targets of mismatch at different extents were examined (Fig. 4B). Obviously, the signal for 1 nM perfectly matched hsa-let-7d-5p (the right column in the histogram) pronounced over the others even the single-base mismatch. Since the devised miRNA sensor has possessed both high sensitivity and satisfactory selectivity, it attempted to determine an emulate human serum as a field trial (Fig. 4C). Compared with the datapoints out of the simple solution (blue sphere), both the background noise and the error bars arise for biological specimens (red triangle). Nevertheless, the developed assay platform substantiates its qualifications for the clinical diagnosis.

3.4. Discussion on DNA hydrogel-based bioassay strategy

This study focused on the synthesis of a new DNA structured hydrogel via dynamic terminus regulation. This technique takes several edges over other existing enzyme-based hydrogelation. First, in principle, it can be interpreted as a cooperation of 3'− end extension and seed-stemmed proliferation. Unlike those jigsaw puzzles from pure hybridization, this concise scheme does not require any template or conserved motif (Goodman et al., 2005; Tjong et al., 2011), yet a comparable goal it can achieve of products at the same scale. Theoretically, replacing dATP with dG/dC-TP would enlarge the DNA network more than ever because of the additive bias in TdT (Sarac and Hollenstein, 2018). Second, such nice transformation efficacy also embodies at those raw materials: flexible initiator and growth factor, homo-polymeric tail of dNTP, and tiny (32 kDa) but active (Michaelis-Menten constant: ~6.7 μM) TdT (Arzumanov et al., 2000), which altogether delivers a robust, versatile, and easy-to-go DNA gel-generating recipe practicable in solutions and on heterogenous surfaces. Third, although TdT works in an indiscriminate style, it is well compatible with dNTP-tethered protein analogues, especially proficient in junctional diversity, the *in situ* localized DNA/RNA labelling, and the rapid amplification of cDNA ends (RACE) (Sarac and Hollenstein, 2018). All in all, the three aspects of hydrogel can serve its miRNA sensing purpose jointly and properly.

Taking advantage of this DNA hydrogel technique, the deter-mination was succeeded in of a clinically rare tumour biomarker miRNA (Su et al., 2016; Wen et al., 2012), which was initiated by the target hybridization on the microelectrode array. Markedly, so low as 0.35 fM miRNA could be measured precisely in the buffer as well as in the human serum. Giving credit to the hydrogel and the patterned 16-channel chip, this approach prevails over the linear duplex-typed fashion at a 5-orders-of-magnitude lower limit, *i.e.* far more sensitivity, and overwhelmingly high throughput (Wan et al., 2014). Still, there are appreciable rooms for improvement on this already outperformance by

timed inactivation on TdT at the cost of additional operations. Notably, the ternary SAMs inside the hydrogel as by-products are able to keep down the background currents to a negligible level (Wu et al., 2010), being offered as an unexpected contribution.

4. Conclusions

In summary, a terminus-controlled DNA fabric was created by the recurring catalytic outreach. Its internal intricacy and gelatin mechanism both were caught a glimpse of by microscopy and electrophoresis. The strategy underlying features high efficiency, easy manipulation, and low cost, which is promising to integrate with microfabrication, DNA nanotechnology and microfluidics for prototyping a unique and potentially useful biointerface. Making the best of synthetic characteristics and enzyme polymerization, an in-situ nucleotide hydrogelation strategy was established for ultrasensitive and highly selective in vitro detection of a special miRNA on the tailored sensor array. This collective and dynamic manipulation of DNA-protein ensembles on interface would infuse fresh new vitality into the ever-developing field of the early diagnostics in disease-related DNA, noncoding RNA and protein markers (by employing aptamers).

Declaration of interests

The authors declare that they have no known competing financial interests or personal relationships that could have appeared to influence the work reported in this paper.

CRediT authorship contribution statement

Shengyuan Deng: Conceptualization, Investigation, Writing - original draft. **Juan Yan:** Methodology, Writing - original draft. **Fei Wang:** Data curation, Investigation. **Yan Su:** Visualization. **Xueli Zhang:** Validation. **Qian Li:** Data curation. **Guang Liu:** Investigation. **Chunhai Fan:** Visualization. **Hao Pei:** Supervision. **Ying Wan:** Writing - review & editing, Supervision.

Acknowledgements

This project was financially supported by the National Natural Science Foundation of China (Grant No. 21874071, 21775072, 21722502, 21775102), Outstanding Youth Foundation of Jiangsu Province (BK20170093), the Fundamental Research Funds for the Central Universities (30916011201, 30916011204, 309171A8803), and Qing Lan Project of Jiangsu Province.

Appendix A. Supplementary data

Supplementary data to this article can be found online at https://doi.org/10.1016/j.bios.2019.04.053.

References

Arzumanov, A.A., Victorova, L.S., Jasko, M.V., Yesipov, D.S., Krayevsky, A.A., 2000. Terminal deoxynucleotidyl transferase catalyzes the reaction of DNA phosphorylation. Nucleic Acids Res. 28 (5), 1276–1281.
Bath, J., Turberfield, A.J., 2007. DNA nanomachines. Nat. Nanotechnol. 2 (5), 275–284.
Fu, Y., Zeng, D., Chao, J., Jin, Y., Zhang, Z., Liu, H., Li, D., Ma, H., Huang, Q., Gothelf, K.V., Fan, C., 2013. Single-step rapid assembly of DNA origami nanostructures for addressable nanoscale bioreactors. J. Am. Chem. Soc. 135 (2), 696–702.
Ge, Z., Lin, M., Wang, P., Pei, H., Yan, J., Shi, J., Huang, Q., He, D., Fan, C., Zuo, X., 2014. Hybridization chain reaction amplification of microRNA detection with a tetrahedral DNA nanostructure-based electrochemical biosensor. Anal. Chem. 86 (4), 2124–2130.
Goodman, R.P., Schaap, I.A., Tardin, C.F., Erben, C.M., Berry, R.M., Schmidt, C.F., Turberfield, A.J., 2005. Rapid Chiral assembly of rigid DNA building blocks. Science 310 (5754), 1661–1665.
Hong, F., Zhang, F., Liu, Y., Yan, H., 2017. DNA origami: scaffolds for creating higher order structures. Chem. Rev. 117 (20), 12584–12640.
Jain, A., Cheng, K., 2017. The principles and applications of avidin-based nanoparticles in drug delivery and diagnosis. J. Control. Release 245, 27–40.
Lee, H.Y., Jeong, H., Jung, I.Y., Jang, B., Seo, Y.C., Lee, H., Lee, H., 2015. DhITACT: DNA hydrogel formation by isothermal amplification of complementary target in fluidic channels. Adv. Mater. 27 (23), 3513–3517.
Lee, J.B., Peng, S., Yang, D., Roh, Y.H., Funabashi, H., Park, N., Rice, E.J., Chen, L., Long, R., Wu, M., Luo, D., 2012. A mechanical metamaterial made from a DNA hydrogel. Nat. Nanotechnol. 7 (12), 816–820.
Li, C., Faulkner-Jones, A., Dun, A.R., Jin, J., Chen, P., Xing, Y., Yang, Z., Li, Z., Shu, W., Liu, D., Duncan, R.R., 2015a. Rapid formation of a supramolecular polypeptide-DNA hydrogel for in situ three-dimensional multilayer bioprinting. Angew Chem. Int. Ed. Engl. 54 (13), 3957–3961.
Li, J., Mo, L., Lu, C.-H., Fu, T., Yang, H.-H., Tan, W., 2016. Functional nucleic acid-based hydrogels for bioanalytical and biomedical applications. Chem. Soc. Rev. 45 (5), 1410–1431.
Li, J., Piehler, L.T., Qin, D., Baker, J.R., Tomalia, D.A., Meier, D.J., 2000. Visualization and characterization of poly (amidoamine) dendrimers by atomic force microscopy. Langmuir 16 (13), 5613–5616.
Li, J., Zheng, C., Cansiz, S., Wu, C., Xu, J., Cui, C., Liu, Y., Hou, W., Wang, Y., Zhang, L., Teng, I.T., Yang, H.H., Tan, W., 2015b. Self-assembly of DNA nanohydrogels with controllable size and stimuli-responsive property for targeted gene regulation therapy. J. Am. Chem. Soc. 137 (4), 1412–1415.
Li, Z., Yin, H., Zhang, Z., Liu, K.L., Li, J., 2012. Supramolecular anchoring of DNA polyplexes in cyclodextrin-based polypseudorotaxane hydrogels for sustained gene delivery. Biomacromolecules 13 (10), 3162–3172.
Liao, W.C., Lilienthal, S., Kahn, J.S., Riutin, M., Sohn, Y.S., Nechushtai, R., Willner, I., 2017. pH-and ligand-induced release of loads from DNA–acrylamide hydrogel microcapsules. Chem. Sci. 8 (5), 3362–3373.
Liu, X., Zhang, F., Jing, X., Pan, M., Liu, P., Li, W., Zhu, B., Li, J., Chen, H., Wang, L., Lin, J., Liu, Y., Zhao, D., Yan, H., Fan, C., 2018. Complex silica composite nanomaterials templated with DNA origami. Nature 559 (7715), 593–598.
Lu, P., Mingxu, Y., Quan, Y., Cuichen, W., Da, H., Yan, C., Zhihua, Z., Jiangeng, X., Weihong, T., 2012. Macroscopic volume change of dynamic hydrogels induced by reversible DNA hybridization. J. Am. Chem. Soc. 134 (29), 12302–12307.
Maffioletti, E., Cattaneo, A., Rosso, G., Maina, G., Maj, C., Gennarelli, M., Tardito, D., Bocchio-Chiavetto, L., 2016. Peripheral whole blood microRNA alterations in major depression and bipolar disorder. J. Affect. Disord. 200, 250–258.
Nagahara, S., Matsuda, T., 1996. Hydrogel formation via hybridization of oligonucleotides derivatized in water-soluble vinyl polymers. Polym. Gels Netw. 4 (2), 111–127.
Pei, H., Lu, N., Wen, Y., Song, S., Liu, Y., Yan, H., Fan, C., 2010. A DNA nanostructure-based biomolecular probe carrier platform for electrochemical biosensing. Adv. Mater. 22 (42), 4754–4758.
Pei, H., Wan, Y., Li, J., Hu, H., Su, Y., Huang, Q., Fan, C., 2011. Regenerable electrochemical immunological sensing at DNA nanostructure-decorated gold surfaces. Chem. Commun. 47 (22), 6254–6256.
Qu, X., Wang, S., Ge, Z., Wang, J., Yao, G., Li, J., Zuo, X., Shi, J., Song, S., Wang, L., Li, L., Pei, H., Fan, C., 2017. Programming cell adhesion for on-chip sequential boolean logic functions. J. Am. Chem. Soc. 139 (30), 10176–10179.
Ratajczak, K., Krazinski, B., Kowalczyk, A., Dworakowska, B., Jakiela, S., Stobiecka, M., 2018a. Optical biosensing system for the detection of survivin mRNA in colorectal cancer cells using a graphene oxide carrier-bound oligonucleotide molecular beacon. Nanomaterials 8 (7), 510.
Ratajczak, K., Krazinski, B.E., Kowalczyk, A.E., Dworakowska, B., Jakiela, S., Stobiecka, M., 2018b. Hairpin–hairpin molecular beacon interactions for detection of survivin mRNA in malignant sw480 cells. ACS Appl. Mater. Interfaces 10 (20), 17028–17039.
Ren, J., Hu, Y., Lu, C.-H., Guo, W., Aleman-Garcia, M.A., Ricci, F., Willner, I., 2015. pH-responsive and switchable triplex-based DNA hydrogels. Chem. Sci. 6 (7), 4190–4195.
Rothemund, P.W., 2006. Folding DNA to create nanoscale shapes and patterns. Nature 440 (7082), 297–302.
Sarac, I., Hollenstein, M., 2018. Terminal deoxynucleotidyl transferase in synthesis and modification of nucleic acids. Chembiochem 20 (7), 860–871.
Seeman, N.C., 2003. DNA in a material world. Nature 421 (6921), 427–431.
Seeman, N.C., 2010. Nanomaterials based on DNA. Annu. Rev. Biochem. 79, 65–87.
Stobiecka, M., Chalupa, A., 2016. DNA strand replacement mechanism in molecular beacons encoded for the detection of cancer biomarkers. J. Phys. Chem. B 120 (21), 4782–4790.
Su, S., Wu, Y., Zhu, D., Chao, J., Liu, X., Wan, Y., Su, Y., Zuo, X., Fan, C., Wang, L., 2016. On-electrode synthesis of shape-controlled hierarchical flower-like gold nanostructures for efficient interfacial DNA assembly and sensitive electrochemical sensing of MicroRNA. Small 12 (28), 3794–3801.
Thomas, T., V, V.N., Jeanette, N., Hao, Y., V, G.K., 2011. DNA origami: a quantum leap for self-assembly of complex structures. Chem. Soc. Rev. 40 (12), 5636–5646.
Tjong, V., Yu, H., Hucknall, A., Rangarajan, S., Chilkoti, A., 2011. Amplified on-chip fluorescence detection of DNA hybridization by surface-initiated enzymatic polymerization. Anal. Chem. 83 (13), 5153–5159.
Um, S.H., Lee, J.B., Park, N., Kwon, S.Y., Umbach, C.C., Luo, D., 2006. Enzyme-catalysed assembly of DNA hydrogel. Nat. Mater. 5 (10), 797–801.
Wan, Y., Wang, P., Su, Y., Wang, L., Pan, D., Aldalbahi, A., Yang, S., Zuo, X., 2015. Nanoprobe-initiated enzymatic polymerization for highly sensitive electrochemical DNA detection. ACS Appl. Mater. Interfaces 7 (46), 25618–25623.
Wan, Y., Wang, P., Su, Y., Zhu, X., Yang, S., Lu, J., Gao, J., Fan, C., Huang, Q., 2014. Ultrasensitive electrochemical DNA sensor based on the target induced structural switching and surface-initiated enzymatic polymerization. Biosens. Bioelectron. 55, 231–236.
Wan, Y., Xu, H., Su, Y., Zhu, X., Song, S., Fan, C., 2013. A surface-initiated enzymatic

polymerization strategy for electrochemical DNA sensors. Biosens. Bioelectron. 41, 526–531.
Wang, P., Wan, Y., Deng, S., Yang, S., Su, Y., Fan, C., Aldalbahi, A., Zuo, X., 2016. Aptamer-initiated on-particle template-independent enzymatic polymerization (aptamer-OTEP) for electrochemical analysis of tumor biomarkers. Biosens. Bioelectron. 86, 536–541.
Wei, B., Dai, M., Yin, P., 2012. Complex shapes self-assembled from single-stranded DNA tiles. Nature 485 (7400), 623–626.
Wei, L., Lei, R., Qian, T., Xiangmeng, Q., Jiang, L., Lihua, W., Li, L., Chunhai, F., Hao, P., 2018. Programming chemical reaction networks using intramolecular conformational motions of DNA. ACS Nano 12 (7), 7093–7099.
Weiwei, G., Xiu-Juan, Q., Ron, O., Chun-Hua, L., Lina, F., Mironi-Harpaz, Iris, D.S., Huang-Hao, Y., Itamar, W., 2014. Reversible Ag + -crosslinked DNA hydrogels. Chem. Commun. 50 (31), 4065–4068.
Wen, Y., Pei, H., Shen, Y., Xi, J., Lin, M., Lu, N., Shen, X., Li, J., Fan, C., 2012. DNA Nanostructure-based Interfacial engineering for PCR-free ultrasensitive electrochemical analysis of microRNA. Sci. Rep. 2, 867.
Winfree, E., Liu, F., Wenzler, L.A., Seeman, N.C., 1998. Design and self-assembly of two-dimensional DNA crystals. Nature 394 (6693), 539–544.
Wu, J., Campuzano, S., Halford, C., Haake, D.A., Wang, J., 2010. Ternary surface monolayers for ultrasensitive (zeptomole) amperometric detection of nucleic acid hybridization without signal amplification. Anal. Chem. 82 (21), 8830–8837.
Xiong, X., Wu, C., Zhou, C., Zhu, G., Chen, Z., Tan, W., 2013. Responsive DNA-based hydrogels and their applications. Macromol. Rapid Commun. 34 (16), 1271–1283.
Yata, T., Takahashi, Y., Tan, M., Hidaka, K., Sugiyama, H., Endo, M., Takakura, Y., Nishikawa, M., 2015. Efficient amplification of self-gelling polypod-like structured DNA by rolling circle amplification and enzymatic digestion. Sci. Rep. 5, 14979.
Zhang, J., Song, S., Wang, L., Pan, D., Fan, C., 2007. A gold nanoparticle-based chronocoulometric DNA sensor for amplified detection of DNA. Nat. Protoc. 2 (11), 2888–2895.
Zhang, L., Lei, J., Liu, L., Li, C., Ju, H., 2013. Self-assembled DNA hydrogel as switchable material for aptamer-based fluorescent detection of protein. Anal. Chem. 85 (22), 11077–11082.
Zhou, G., Lin, M., Song, P., Chen, X., Chao, J., Wang, L., Huang, Q., Huang, W., Fan, C., Zuo, X., 2014. Multivalent capture and detection of cancer cells with DNA nanostructured biosensors and multibranched hybridization chain reaction amplification. Anal. Chem. 86 (15), 7843–7848.